NANO LETTERS
2005
Vol. 5, No. 12
2426−2431

Nanotechnology-Based Photodynamic Therapy for Neovascular Disease Using a Supramolecular Nanocarrier Loaded with a Dendritic Photosensitizer

Ryuichi Ideta,[†,‡] Fumitaka Tasaka,[†,‡,▽] Woo-Dong Jang,[†,§] Nobuhiro Nishiyama,[∥] Guo-Dong Zhang,[§] Atsushi Harada,[⊥] Yasuo Yanagi,[‡] Yasuhiro Tamaki,[‡] Takuzo Aida,[#] and Kazunori Kataoka*[,§,∥]

Department of Ophthalmology, Graduate School of Medicine, The University of Tokyo, 7-3-1 Hongo, Bunkyo-ku, Tokyo 113-8655, Japan, Department of Materials Science and Engineering, Graduate School of Engineering, The University of Tokyo, 7-3-1 Hongo, Bunkyo-ku, Tokyo 113-8656, Japan, Center for Disease Biology and Investigative Medicine, Graduate School of Medicine, The University of Tokyo, 7-3-1 Hongo, Bunkyo-ku, Tokyo 113-0033, Japan, Department of Applied Materials Science, Graduate School of Engineering, Osaka Prefecture University, 1-1 Gakuen-cho, Sakai, Osaka 599-8531, Japan, Department of Chemistry and Biotechnology, Graduate School of Engineering, The University of Tokyo, 7-3-1 Hongo, Bunkyo-ku, Tokyo 113-8656, Japan, and Research & Development Division, Santen Pharmaceutical Co., Ltd., 8916-16 Takayama-cho, Ikoma, Nara 630-0101, Japan

Received August 23, 2005; Revised Manuscript Received October 3, 2005

ABSTRACT

Photodynamic therapy (PDT) for exudative age-related macular degeneration (AMD) was evaluated using a supramolecular nanomedical device, that is, a novel dendritic photosensitizer (DP) encapsulated by a polymeric micelle formulation. The characteristic dendritic structure of the DP prevents aggregation of its core sensitizer, thereby inducing a highly effective photochemical reaction. With its highly selective accumulation on choroidal neovascularization (CNV) lesions, this treatment resulted in a remarkably efficacious CNV occlusion with minimal unfavorable phototoxicity.

Photodynamic therapy (PDT) is one of the noninvasive ways of treating malignant tumors or macular degeneration.[1] PDT is based on the delivery of a photosensitizer (PS) to the target tissue after the administration of PS. Photoirradiation by appropriate laser light generates highly reactive oxygen species, such as singlet oxygen, which results in the oxidative destruction of target tissue. There are several kinds of already developed PSs for the clinical evaluation of their photodynamic efficacy. Most of the conventional PSs have large π-conjugation domains to extend their absorption cross sections and basically have hydrophobic characteristics. Therefore, PSs form aggregates easily, which produce the self-quenching of the excited state, in aqueous medium because of their $\pi-\pi$ interaction and hydrophobic characteristics. To improve the photodynamic efficacy, the efficient delivery of PSs and high quantum yield of the singlet oxygen generation are significantly important. On the basis of this information, we have reported a dendrimer-based PS recently, dendrimer porphyrin (DP),[2−4] in which the focal porphyrin is surrounded by the third generation of poly(benzyl ether) dendrons (Figure 1a).[5] Unlike conventional PSs, the DP ensures the efficacy of singlet oxygen production even at an extremely high concentration because the dendritic

* Corresponding author. Address: Department of Materials Science and Engineering, Graduate School of Engineering, The University of Tokyo, 7-3-1 Hongo, Bunkyo-ku, Tokyo 113-8656, Japan. Fax +81-3-5841-7139. Tel +81-3-5841-7138. E-mail: kataoka@bmw.t.u-tokyo.ac.jp.
[†] Equally contributed to this work.
[‡] Department of Ophthalmology, Graduate School of Medicine, The University of Tokyo.
[§] Department of Materials Science and Engineering, Graduate School of Engineering, The University of Tokyo.
[∥] Center for Disease Biology and Investigative Medicine, Graduate School of Medicine, The University of Tokyo.
[⊥] Osaka Prefecture University.
[#] Department of Chemistry and Biotechnology, Graduate School of Engineering, The University of Tokyo.
[▽] Santen Pharmaceutical Co., Ltd.

10.1021/nl051679d CCC: $30.25
Published on Web 10/27/2005

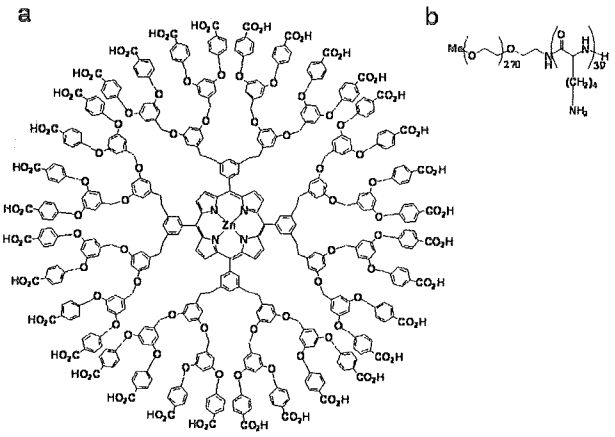

Figure 1. Structures of DP (a) and poly(ethylene glycol)-*block*-poly(L-lysine) (PEG-b-P(Lys) (b).

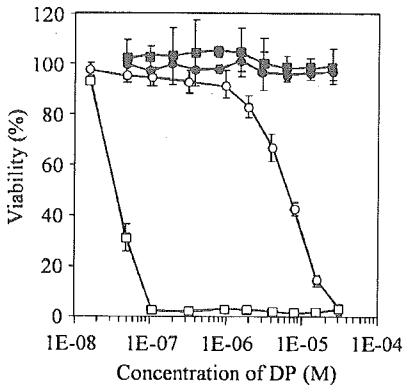

Figure 2. In vitro cytotoxicity of free DP (circle) and DP-loaded micelle (square) in the presence (open symbol) or absence (closed symbol) of photoirradiation. Encapsulation of DP into the micelle resulted in a 280-fold increase in the phototoxicity in vitro.

envelope of DP can prevent aggregation of the central porphyrin.[6] Also, the 32 negative charges on DP allow its stable incorporation into a supramolecular nanocarrier, the polyion complex (PIC) micelle,[7] through electrostatic interaction with oppositely charged block copolymers (Figure 1b).[8,9]

Alternatively, age-related macular degeneration (AMD), a condition caused by choroidal neovascularization (CNV), is a major cause of legal blindness in developed countries. Recently, large randomized control studies demonstrated that PDT with Visudyne, a liposomal formulation of verteporfin, prevents severe visual loss due to CNV and was approved for clinical use.[10,11] However, because of the intractableness of AMD, most patients require repeated treatments every three months, still suffering from a reduced quality of life.[12] It should also be noted that even with the repeated PDT treatment, most patients end in visual loss because of recurring CNV,[13] thus prompting investigators to search for alternative PSs with even higher PDT efficacies. For effective PDT against AMD, the selective delivery of PS to the CNV lesions and an effective photochemical reaction at the CNV sites is necessary. In regard to the delivery of PS, low-density lipoproteins and antibodies against endothelial cell markers have been used as carrier molecules;[14] however, PS also distributes to normal vessels to some extent because normal vessels also express such markers. In addition, as described previously, the increased loading of PSs to drug vehicles could change the photochemical reaction mechanism from type II to type I because of the formation of aggregates, leading to a diminished photodynamic efficacy.[15] Thus, there is a strong impetus to develop novel PS formulations from the standpoint of both the efficiency of the delivery and photochemical reactions of the PS itself. Herein, we report the first example of the in vivo evaluation of dendritic PS for PDT treatment against AMD and wish to highlight the selective accumulation and photodynamic effect of the DP-loaded micelle on the CNV lesions.

Before the in vivo experiment, the photoinduced cytotoxic property of DP and the DP-loaded micelle was evaluated against Lewis lung cells, where the DP-loaed micelle was prepared as follows. A negatively charged third-generation ionic DP having 32 carboxylate end groups and PEG-b-P(Lys) was prepared by a method reported previously.[8] The PEG-b-P(Lys) was dissolved in aqueous NaH_2PO_4 (10 mM, pH = 4.95) and added to an aqueous solution of DP in Na_2HPO_4/0.1 N NaOH (10 mM Na_2HPO_4, pH = 11.54) to give a solution (10 mM, pH = 7.30) containing DP-loaded micelles, in which the molar ratio of the carboxylate end groups and lysine residues was adjusted to unity. The prepared PIC micelle had a unimodal size distribution. As shown in Figure 2, neither the DP nor DP-loaded micelle exhibit any toxic profiles under a dark condition, whereas either the DP or DP-loaded micelle shows a strong cytotoxicity under light irradiation. Notably, the encapsulation of DP into the micelle resulted in a 280-fold increase in the phototoxicity.

In an attempt to deliver PS to the CNV sites, a free DP and a DP-loaded PIC micelle were examined. To investigate the accumulation of the DP-loaded micelles encapsulating DP in the CNV lesions, we created experimental CNV as follows.[16] A general anesthesia was induced with an intraperitoneal injection (1000 μL/kg) of a mixture (7:1) of ketamine hydrochloride (Ketalar, Sankyo, Tokyo, Japan) and xylazine hydrochloride (Celactal, Bayer, Tokyo, Japan) or by the inhalation of diethyl ether. The pupil was dilated with one drop of 0.5% tropicamide (Mydrin M, Santen Pharmaceutical, Osaka, Japan) for photocoagulation. Four laser photocoagulations were applied to each eye of 16 rats (Male Brown Norway (BN) rats, 60−80 g, Saitama Animal Lab., Inc., Saitama, Japan) between the major retinal vessels around the optic disk with a diode-laser photocoagulator (DC-3000®, NIDEK, Osaka, Japan) and a slit lamp delivery system (SL150, Topcon, Tokyo, Japan) at a spot size of 75 μm, duration of 0.05 s, and intensity of 300 mW. By tail vein injection, 400 μL of the DP-loaded micelle encapsulating 1.5 mg/mL DP or 400 μL of free DP (1.5 mg/mL) was administered into rats 7 days after the photocoagulation. After the rats were sacrificed with an overdose of sodium pentobarbital, the eyes were enucleated immediately and snap-frozen in OCT compound 0.25, 1, 4, and 24 h later for the

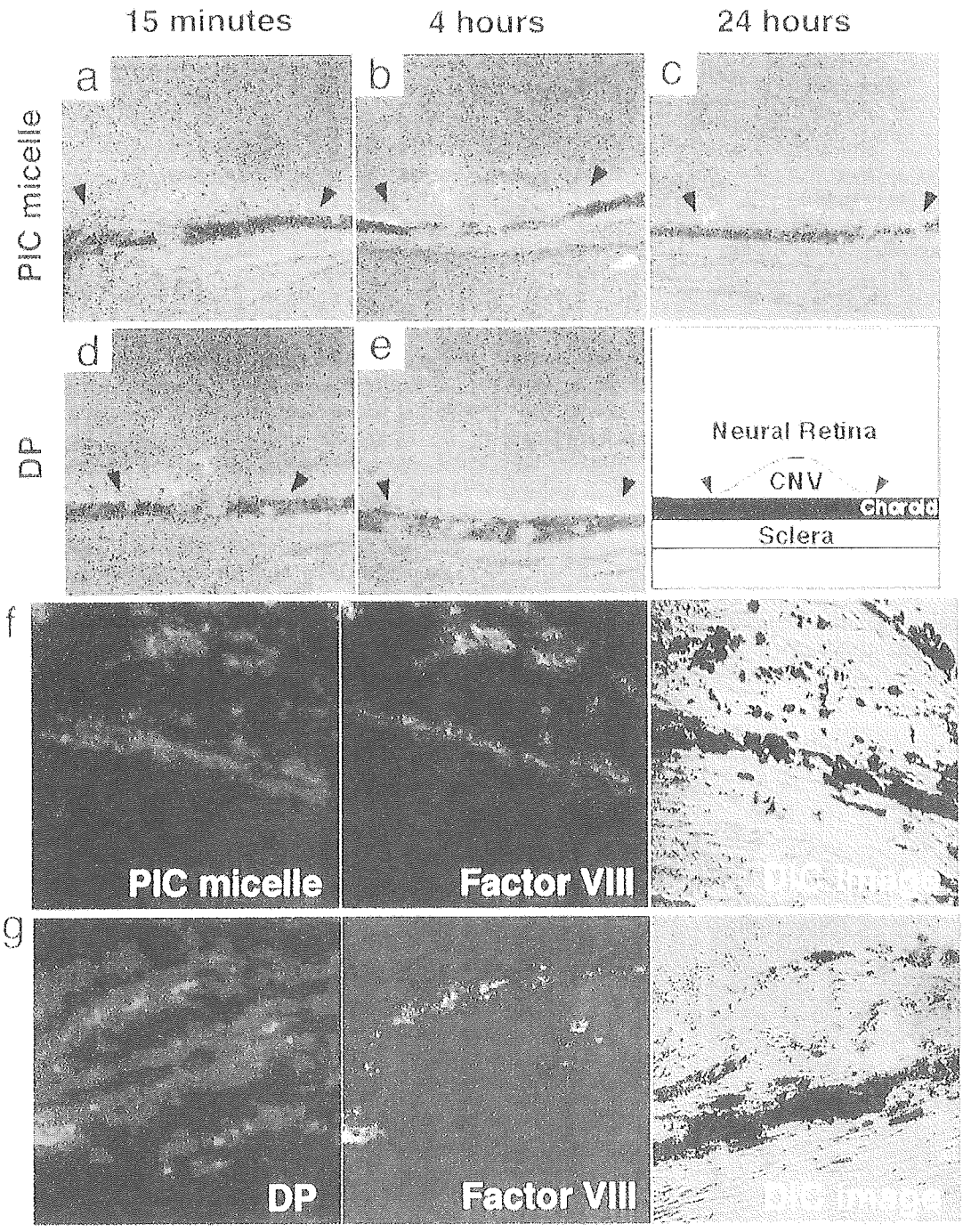

Figure 3. Accumulation of DP after administration of DP-loaded micelles to rats with experimental CNV (a–e). Accumulation of the DP-loaded micelle (a–c) and free DP (d and e) to experimental CNV. When the DP-loaded micelle was administered, the accumulation of DP in CNV lesions was observed as early as 15 min after the injection, peaked at 4 h, and was still evident 24 h after the injection. Whereas, after the free DP injection, DP was also present in CNV lesions for up to 4 h, but disappeared within 24 h (f and g). Immunohistochemistry shows the localization of the micelle and DP and factor VIII-positive endothelial cells. Note that DP is present within the factor VIII-positive endothelial cells when the DP-loaded micelle is administered, whereas DP was present mainly outside the factor VIII-positive endothelial cells when free DP was administered.

PIC micelle group ($n = 4$ at each time point) and 1 h later for the free DP group ($n = 4$). The frozen sections were mounted using the ProLong Antifade Kit (Molecular Probes, Eugene, Oregon) and observed under a fluorescent microscope (model IX, Olympus, Tokyo, Japan). Interestingly, the results showed an effective and selective accumulation of the micelle in the CNV lesions, indicating that the CNV lesions may have characteristic features similar to solid tumor vasculatures, such as hyperpermeability and impaired lymphatic drainage (i.e., so-called EPR effect[17]).[18–21] The

Table 1. CNV Closure Rate (%) after PDT

PDT condition	observation days	light fluence 0 J/cm^2	5 J/cm^2	50 J/cm^2
control	1	31.7 ± 13.4		
	7	15.0 ± 3.5		
treatment at 0.25 h after DP administration	1	20.9 ± 4.2	19.4 ± 5.6	20.8 ± 4.2
	7	25.0 ± 8.3	33.3 ± 8.3	18.8 ± 2.1
treatment at 0.25 h after DP-loaded micelle administration	1	33.3 ± 0	77.7 ± 5.6	77.1 ± 2.9
	7	25.0 ± 8.3	80.5 ± 2.8	83.4 ± 5.2
treatment at 4 h after DP-loaded micelle administration	1	33.3 ± 0	60.0 ± 10.0	72.2 ± 15.5
	7	25.0 ± 8.3	81.7 ± 1.7	77.8 ± 2.8

accumulation of DP in the CNV lesions was observed by histological analysis. For the histological analysis, prepared frozen sections were stained with FITC-conjugated monoclonal antibody against factor VIII (Dako cytomation, San Diego, CA), mounted with the ProLong Antifade Kit (Molecular Probes, Eugene, Oregon), and observed under a fluorescent microscope (model IX, Olympus, Tokyo, Japan). Both the free DP and DP-loaded micelles were recruited clearly in the CNV lesions (Figure 3a–e).

However, they exhibited drastically different aspects of accumulation. When the DP-loaded micelle was administered, the accumulation of DP to the CNV lesions was observed as early as 15 min after the injection, peaked at 4 h, and was still evident 24 h after the injection. Interestingly, the immunohistochemical analysis demonstrated that DP was present within the factor VIII-positive endothelial cells when the DP-loaded micelle was administered (Figure 3f). In contrast, after the free DP injection, DP concentrated in the CNV lesion up to 4 h (Figure 3d and e) but disappeared within 24 h. The immunohistochemical analysis demonstrated that DP was present not only in the factor VIII-positive endothelial cells but also outside of those cells when compared to the DP-loaded micelle administration (Figure 3g). These observations agree with our previous finding in vitro that the free DP exhibits a lowered cellular uptake because of its negatively charged periphery.[3] Therefore, the

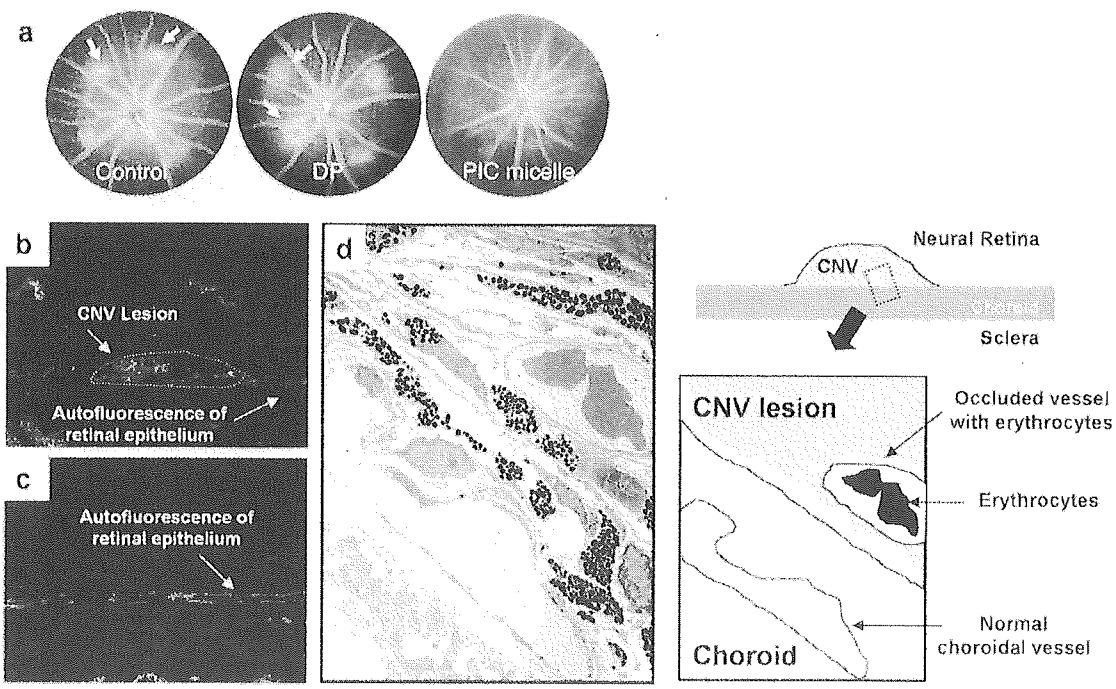

Figure 4. Efficacy of PDT laser after administration of the DP-loaded micelle. (a) Representative images of fluorescein angiograms in control, PDT-laser-irradiated eye after free DP was administered (DP), and PDT-laser-irradiated eye after the DP-loaded micelle was administered (PIC micelle). Note that the enhanced accumulation of DP-loaded micelles in CNV lesions resulted in a significantly pronounced photodynamic effect, whereas almost all of the CNV lesions showed a strong hyperfluorescence (marked with arrows), and the CNV endothelial cells appeared normal when free DP was administered. (b) Immunostaining of the endothelial cells with factor VIII antibody. Strong fluorescence from the CNV lesion is observable. (c) Immunostaining of the endothelial cells with factor VIII antibody after PDT treatment with DP-loaded micelle. Note that CNV lesion is occluded, and only autofluorescence from retinal pigment epithelium is observable. (d) Transmission electron microscopy of the CNV lesion of the PDT laser-irradiated eye after the DP-loaded micelle was administered. The neovascular blood vessel in CNV lesion is occluded by erythrocytes, whereas the normal choroidal vessel is not destroyed.

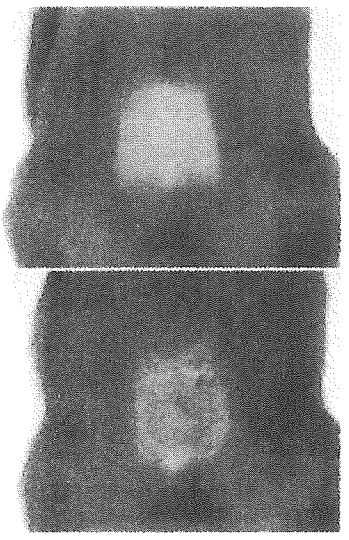

Figure 5. Macroscopic skin phototoxicity of DP-loaded micelle (top panel) and Photofrin (bottom panel). Skin phototoxicity was not observed macroscopically when the rats were exposed to broadband visible light 4 h after the injection of a DP-loaded micelle, whereas a severe phototoxicity was observed after the injection of Photofrin.

DP-loaded micelle is a very effective vehicle for delivery to factor VIII-positive endothelial cells for efficient photodynamic treatment.

Indeed, the enhanced accumulation of the micelle-encapsulated DP into CNV lesions resulted in a significantly pronounced photodynamic effect, which was evaluated using fluorescein angiography. When the PDT laser was applied 15 min after the injection of a DP-loaded micelle, 78% of the CNV lesions showed no fluorescein leakage at day 1 (Table 1). At day 7, the hypofluorescence persisted (Table 1), suggesting that leakage from the CNV lesions was still reduced. Similar results were observed when PDT was performed 4 h after the injection (Table 1). In sharp contrast, neither the administration of DP alone nor the application of the PDT laser alone affected the CNV activity (i.e., a similar proportion of the CNV lesions showed leakage (ca. 20−30% closure rate; Table 1, Figure 4a)).

Immunohistochemical analysis with factor-VIII demonstrated that CNV endothelial cells were destroyed by the PDT laser compared to the untreated control lesion when the lesion was treated with the laser after the administration of a DP-loaded micelle (Figure 4b and c). Transmission electron microscopy revealed that the vessels in the CNV lesion regressed to collagen tubes without endothelial cells or were occluded by erythrocytes (Figure 4d). Importantly, the endothelial cells of the overlying normal blood vessel in the retina and choroid in the treated lesions were not destroyed, even after the application of the PDT laser at maximum energy after the administration of the DP-loaded micelle, probably because neither the PIC micelle nor free DP was taken up into the endothelial cells in normal blood vessels. Moreover, as shown in Figure 5, skin phototoxicity is not macroscopically observable when the rats were exposed to broadband visible light (Xenon lamp equipped with a filter passing light of 377−700 nm, incident light irradiance; approximately 30 mW/cm^2) 4 h after the injection of the DP-loaded micelle (400 μL, 1.5 mg/mL), which is in sharp contrast to the results observed after the injection of a clinically used PS formulation, Photofrin (400 μL, 1.5 mg/mL). In contrast to the suppressive effect after the administration of the DP-loaded micelle, almost all of the CNV lesions showed a strong hyperfluorescence (i.e., no occlusion of CNV) and the CNV endothelial cells appeared normal when free DP was applied under identical PDT conditions (Figure 4a and Table 1). In addition, as described previously, the encapsulation of DP into the micelle resulted in a 280-fold increase in phototoxicity. Because the DP-loaded micelle is assumed to dissociate gradually into the constituent DP and block copolymer in the body by dilution, long-term phototoxicity is avoidable after PDT using this micelle.

In the present paper, a novel concept for the treatment of CNV using the combination of a dendrimer photosensitizer and polymeric micelles was presented. The DP-loaded micelle achieved a highly selective accumulation of DP in the CNV lesions, and a lower power energy of light was sufficient to occlude the CNV lesions. This might be attributed to the unique characteristic of DP; the aggregation of the core porphyrin is sterically prevented even at a remarkably high concentration. Our data suggest that the DP-loaded micelles enhanced the efficacy of PDT significantly while circumventing side effects to the normal retinal and choroidal vessels and skin. Also, this protocol is applicable to the PDT of solid tumors. From the standpoint of the clinical use for solid tumors, we are developing dendritic PSs with longer excitation wavelengths currently. Nevertheless, our results strongly suggest the usefulness of dendritic PSs and their micellar formulation for effective PDT. The data in this communication will provide a novel paradigm for practical use in biomedical fields as dendrimer-based nanomedicines.

Acknowledgment. This study was supported by Industrial Technology Research Grant Program in 2004 from New Energy and Industrial Technology Development Organization (NEDO) of Japan and partially supported by the Core Research for Evolutional Science and Technology (CREST) from the Japan Science and Technology Agency (JST).

References

(1) Pandey, R. K.; Zhang, G. *Porphyrin Handbook*; Kadish, K. M., Smith, K. M., Guilard, R., Eds.; Academic Press: San Diego, CA, 2000; Vol. 6.
(2) Tomioka, N.; Takasu, D.; Takahashi, T.; Aida, T. *Angew. Chem., Int. Ed.* **1998**, *37*, 1531.
(3) Jang, W.-D.; Nishiyama, N.; Zhang, G.-D.; Harada, A.; Jiang, D.-L.; Kawauchi, S.; Morimoto, Y.; Kikuchi, M.; Koyama, H.; Aida, T.; Kataoka, K. *Angew. Chem., Int. Ed.* **2005**, *44*, 419.
(4) Nishiyama, N.; Stapert, H. R.; Zhang, G.-D.; Takasu, D.; Jiang, D.-L.; Nagano, T.; Aida, T.; Kataoka, K. *Bioconjugate Chem.* **2003**, *14*, 58.
(5) Hawker, C. J.; Frechet, J. M. J. *J. Am. Chem. Soc.* **1990**, *112*, 7638.
(6) Sato, T.; Jiang, D.-L.; Aida, T. *J. Am. Chem. Soc.* **1999**, *121*, 10658.
(7) Harada, A.; Kataoka, K. *Science* **1999**, *283*, 65.
(8) Harada, A.; Kataoka, K. *Macromolecules* **1995**, *28*, 5294
(9) Stapert, H. R.; Nishiyama, N.; Jiang, D.-L.; Aida, T.; Kataoka, K. *Langmuir* **2000**, *16*, 8182.

(10) Bressler, N. M.; Arnold, J.; Benchaboune, M.; Blumenkranz, M. S.; Fish, G. E.; Gragoudas, E. S.; Lewis, H.; Schmidt-Erfurth, U.; Slakter, J. S.; Bressler, S. B.; Manos, K.; Hao, Y.; Haynes, L.; Koester, J.; Reaves, A.; Strong, H. A. *Arch. Ophthalmol.* **2002**, *120*, 1443.
(11) Ferris, F. L.; Fine, S. L.; Hyman, L. *Arch. Ophthalmol.* **1984**, *102*, 1640.
(12) Meads, C.; Hyde, C. *Br. J. Ophthalmol.* **2004**, *88*, 212.
(13) Wormald, R.; Evans, J.; Smeeth, L.; Henshaw, K. *Cochrane Database Syst. Rev.* **2003**, CD002030.
(14) Renno, R. Z.; Miller, J. W. *Adv. Drug Delivery Rev.* **2001**, *52*, 63.
(15) Grossweiner, L. I.; Patel, A. S.; Grossweiner, J. B. *Photochem. Photobiol.* **1982**, *36*, 159.
(16) Yanagi, Y. *Invest. Ophthalmol. Visual Sci.* **2003**, *44*, 751.
(17) Matsumura, Y.; Maeda, H. *Cancer Res.* **1986**, *46*, 6387.
(18) Nishiyama, N.; Okazaki, S.; Cabral, H.; Miyamoto, M.; Kato, Y.; Sugiyama, Y.; Nishio, K.; Matsumura, Y.; Kataoka, K. *Cancer Res.* **2003**, *63*, 8977.
(19) Kwon, G.; Suwa, S.; Yokoyam, M.; Okano, M.; Sakurai, Y.; Kataoka, K. *J. Controlled Release* **1994**, *29*, 17−23.
(20) Yokoyama, M.; Okano, T.; Sakuraj, Y.; Fukushima, S.; Okamoto, K.; Kataoka, K. *J. Drug Target.* **1999**, *7*, 171.
(21) Ideta, R.; Yanagi, Y.; Tamaki, Y.; Tasaka, F.; Harada, A.; Kataoka, K. *FEBS Lett.* **2004**, *557*, 21.
(22) Boas, U.; Heegaard, P. M. H. *Chem. Soc. Rev.* **2004**, *33*, 43.

NL051679D

Effective accumulation of polyion complex micelle to experimental choroidal neovascularization in rats

Ryuichi Ideta[a,1], Yasuo Yanagi[a,*], Yasuhiro Tamaki[a], Fumitaka Tasaka[a,b,1], Atsushi Harada[c], Kazunori Kataoka[d]

[a] *Department of Ophthalmology, University of Tokyo School of Medicine, 7-3-1 Hongo, Bunkyo-ku, Tokyo 113-8655, Japan*
[b] *Research and Development Division, Santen Pharmaceutical Co., Ltd., 8916-16 Takayama-cho, Ikoma, Nara 630-0101, Japan*
[c] *Department of Applied Materials Science, Graduate School of Engineering, Osaka Prefecture University, 1-1 Gakuen-cho, Sakai, Osaka 599-8531, Japan*
[d] *Department of Materials Science and Engineering, Graduate School of Engineering, The University of Tokyo, 7-3-1 Hongo, Bunkyo-ku, Tokyo 113-8656, Japan*

Received 26 September 2003; revised 6 November 2003; accepted 7 November 2003

First published online 22 December 2003

Edited by Guido Tettamanti

Abstract Exudative age-related macular degeneration, characterized by choroidal neovascularization (CNV), is a major cause of visual loss. In this study, we examined the distribution of the polyion complex (PIC) micelle encapsulating FITC-P(Lys) in blood and in experimental CNV in rats to investigate whether PIC micelle can be used for treatment of CNV. We demonstrate that PIC micelle has long-circulating characteristics, accumulating to the CNV lesions and is retained in the lesion for as long as 168 h after intravenous administration. These results raise the possibility that PIC micelles can be used for achieving effective drug targeting to CNV.

Key words: Age-related macular degeneration; Choroidal neovascularization; Drug delivery system; Nanotechnology; Polyion complex micelle

1. Introduction

Exudative age-related macular degeneration (AMD), characterized by choroidal neovascularization (CNV), is a major cause of visual loss in developed countries [1,2]. Photocoagulation of the entire CNV is an effective treatment option for exudative AMD proved in large randomized control studies performed by the Macular Photocoagulation Study Group [3]. However, since most CNV extends to the subfovea, permanent central visual loss is inevitable immediately after photocoagulation. Thus, alternative treatments for CNV with minimal damage to the healthy retina, such as photodynamic therapy, are being developed [4]. In addition, compounds with anti-angiogenic properties are under intensive study for possible clinical applications [5,6]. Although studies in vivo using animal CNV models have demonstrated the favorable results of several anti-angiogenic drugs such as interferon-β and thalidomide, these drugs were not effective in inhibiting the development of CNV in humans. To develop a pharmacological therapy for CNV with minimal systemic adverse effects, it is necessary to achieve a high local concentration of the drug [7].

These results have prompted the search for an alternative drug delivery system. Macromolecules can accumulate and prolong their retention in perivascular regions of solid tumors to a greater extent than in normal tissues because newly formed vessels in solid tumors exhibit high substance permeability compared with those in normal tissues, and the lymph systems in tumor tissue are incomplete [8,9]. This effect is known as the enhanced permeability retention (EPR) effect [10]. CNV membranes have high permeability and several studies have demonstrated that macromolecules accumulate in experimental CNV presumably through the EPR effect [7].

The size of the molecules is an important factor in exerting the EPR effect. Polymeric micelles have a size range of several tens of nanometers with a very narrow distribution, similar to that of viruses and lipoproteins [8]. Thus, they accumulate in solid tumors through the EPR effect [11,12]. In addition, compared with the drug delivery system based on macromolecule conjugates, polymeric micelle can stably encapsulate chemical compounds with high efficiency [8]. On the basis on this together with their high drug-loading capacity, polymeric micelles are expected to become a novel drug delivery system. In fact, we have developed a drug delivery system with polymeric micelles encapsulating doxorubicin [13] and it is now in phase II clinical trial for the treatment of solid tumors [14].

We have recently developed a novel type of polymeric micelle formed through electrostatic interaction (polyion complex (PIC) micelle) [8,15]. Unlike polyion complexes formed from an oppositely charged pair of simple homopolymers or statistical copolymers, PIC micelles from charged block copolymers are totally water-soluble and are narrowly distributed. In this study, to investigate whether PIC micelle can be used for treatment of CNV, we examined the distribution of the PIC micelle in blood and in experimental CNV in rats.

*Corresponding author. Fax: (81)-3-3817 0798.
E-mail address: yanagi-tky@umin.ac.jp (Y. Yanagi).

[1] These authors contributed equally to this work.

Abbreviations: AMD, age-related macular degeneration; CNV, choroidal neovascularization; DLS, dynamic light scattering; EPR, enhanced permeability retention; PIC, polyion complex

0014-5793/03/$30.00
doi:10.1016/S0014-5793(03)01315-2

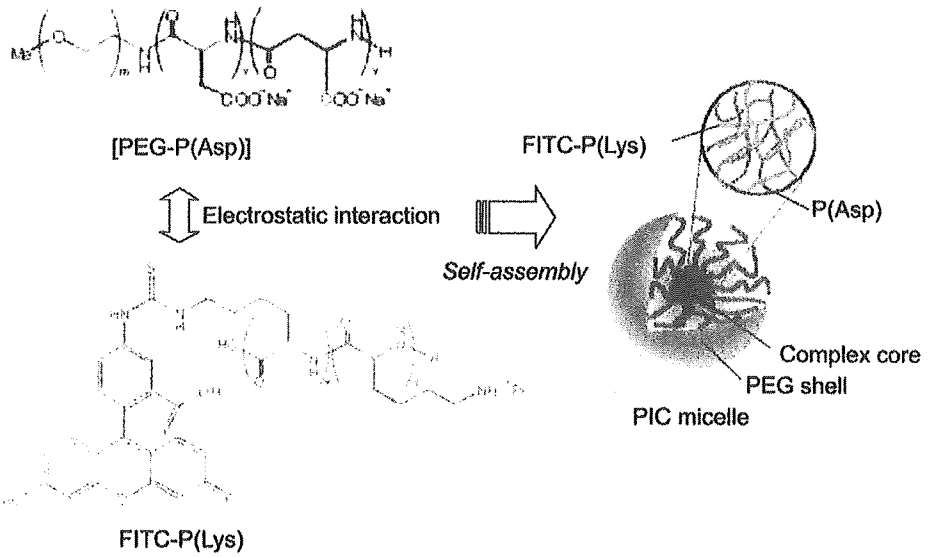

Fig. 1. Preparation and schematic structure of PIC micelle encapsulating FITC-P(Lys). PIC micelle consists of an inner complex core formed by the P(Asp) segment and FITC-P(Lys), and an outer PEG shell.

2. Materials and methods

2.1. Animals

Male Brown Norway rats weighing 100–120 g were obtained from Saitama Animal Lab (Saitama, Japan). All experiments were conducted in accordance with the Animal Care and Use Committee and the Association for Research in Vision and Ophthalmology Statement for the Use of Animals in Ophthalmic and Vision Research.

2.2. Experimental CNV

A general anesthesia was induced with an intraperitoneal injection (1000 μl/kg) of a mixture (7:1) of ketamine hydrochloride (Ketalar®, Sankyo, Tokyo, Japan) and xylazine hydrochloride (Celactal®, Bayer, Tokyo, Japan) or by inhalation of diethyl ether. The pupil was dilated with one drop of 0.5% tropicamide (Mydrin® M, Santen Pharmaceutical, Osaka, Japan) for photocoagulation. Experimental CNV was created as previously described [16,17]. Fifty laser photocoagulations were applied to each eye between the major retinal vessels around the optic disc with a diode laser photocoagulator (DC-3000®, Nidek, Osaka, Japan) and a slit lamp delivery system (SL150, Topcon, Tokyo, Japan) at a spot size of 75 μm, duration of 0.05 s, and intensity of 200 mW.

2.3. Preparation of PIC micelle encapsulating fluorescein isothiocyanate-labeled poly-L-lysine (Fig. 1)

Fluorescein isothiocyanate-labeled poly-L-lysine [FITC-P(Lys), 100.0 mg; polymerization degree = 105, FITC = 0.004 mol/mol of Lys] and 48.6 mg of polyethylene glycol-*block*-poly-α,β-aspartic acid) [PEG-P(Asp); PEG MW = 5000 g/mol, polymerization degree of P(Asp) segment = 78] were dissolved in 10.0 and 5.0 ml of phosphate-buffered saline (PBS), respectively. PIC micelle solution was prepared by mixing the same volume (5.0 ml) of FITC-P(Lys) and PEG-P(Asp) solutions, in which the molar ratio of Lys and Asp residues was adjusted to unity. As a control, 5.0 ml of FITC-P(Lys) solution was diluted in 5.0 ml of PBS. Both PIC micelle and control solutions included the same concentration (5.0 mg/ml) of FITC-P(Lys). The average diameter and polydispersity index of PIC micelles was evaluated by dynamic light scattering (DLS) measured at 25°C, using a light scattering spectrophotometer (DLS-7000, Otsuka Electronics, Osaka, Japan) with a vertically polarized incident beam at 632.8 nm supplied by a He/Ne laser. A scattering angle of 90° was used in this study.

2.4. Accumulation of PIC micelle to CNV lesions: histological analysis

To investigate the accumulation of PIC micelle to the CNV lesions, 50 photocoagulations were applied to the right eye of a total of 23 rats. The left eyes served as non-photocoagulation controls. By tail injection, 400 μl of PIC micelle encapsulating 5.0 mg/ml FITC-P(Lys) or 400 μl of free FITC-P(Lys) at a concentration of 5.0 mg/ml ($n = 3$) was administered to rats 7 days after photocoagulation. There was high mortality in rats receiving FITC-P(Lys) after 1 h, suggesting that P(Lys) has toxicity.

After the rats were killed with an overdose of sodium pentobarbital, the eyes were immediately enucleated, snap-frozen in OCT compound 1, 4, 8, 24, and 168 h later for the PIC micelle group ($n = 4$ at each time point) and 1 h later for the FITC P(Lys) group ($n = 3$). Then frozen sections were mounted with the ProLong Antifade Kit (Molecular Probes, Eugene, OR, USA) and observed under a fluorescent microscope (model IX, Olympus, Tokyo, Japan).

2.5. Measurement of the concentration of PIC micelle in laser-treated eyes and blood

To investigate the concentration of FITC-P(Lys) in laser-treated eyes and blood, rats received PIC micelle encapsulating FITC-

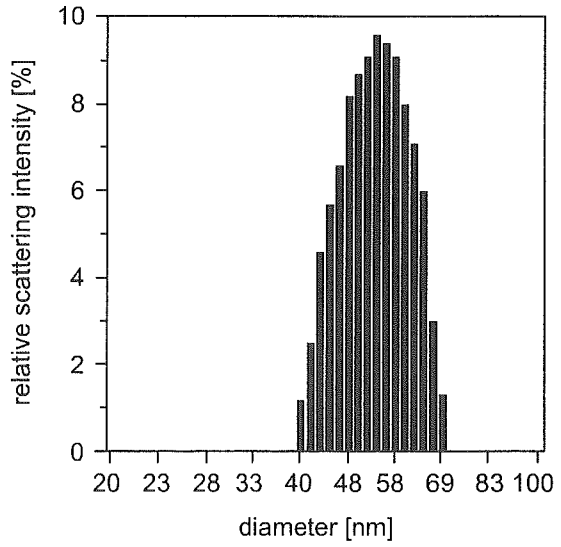

Fig. 2. DLS histogram of PIC micelle encapsulating FITC-P(Lys). The average diameter and polydispersity index of PIC micelles were evaluated by DLS measurement at 25°C, using a light scattering spectrophotometer. PIC micelle was narrowly dispersed with a size around 50.7 nm.

P(Lys) ($n = 20$) or free FITC-P(Lys) ($n = 3$) intravenously 7 days after photocoagulation. They were killed with an overdose injection of sodium pentobarbital 1, 4, 8, 24 and 168 h after receiving the PIC micelles encapsulating FITC-P(Lys) ($n = 4$ at each time point) and 1 h after receiving free FITC-P(Lys) ($n = 3$). Immediately after death, blood samples were collected and the eyes were enucleated. The blood samples were centrifuged at 12 000 rpm for 5 min and the supernatant was collected and subjected to spectrophotometric analysis. The retina/choroid was collected after the anterior segment and vitreous were removed. Then, the retina/choroid samples were homogenized in 0.1 ml of PBS and suspended in a total of 0.3 ml of PBS. The homogenates were then centrifuged at 12 000 rpm for 5 min and the supernatant was collected and subjected to spectrophotometric analysis. The fluorescence intensity was measured in a fluorescence spectrophotometer (FP-6500, Jasco, Tokyo, Japan) with an excitation wavelength of 495 nm and an emission wavelength of 520 nm. The actual concentration of FITC-P(Lys) was calculated by means of a calibration curve.

2.6. Statistical analysis

Mann–Whitney's *U*-test was used. Values of $P < 0.05$ were considered statistically significant.

3. Results

3.1. Preparation of PIC micelle encapsulating FITC-P(Lys)

Precipitation after mixing FITC-P(Lys) and PEG-P(Asp) solutions at 25°C was not observed, even after a period of over 2 months, suggesting the high storing stability of PIC micelle. Fig. 2 shows the size distribution of PIC micelle obtained from histogram analysis of DLS measurements. It was clear that the prepared PIC micelle had a unimodal size distribution. Also the average diameter and polydispersity index of PIC micelle were determined to be 50.7 nm and 0.046 by using the cumulant approach of DLS measurement, indicating the formation of PIC micelle with an extremely narrow size distribution.

3.2. Accumulation of PIC micelle to CNV lesions

3.2.1. PIC micelle group. Fluorescent staining was observed in the CNV lesions and also in the choriocapillaris

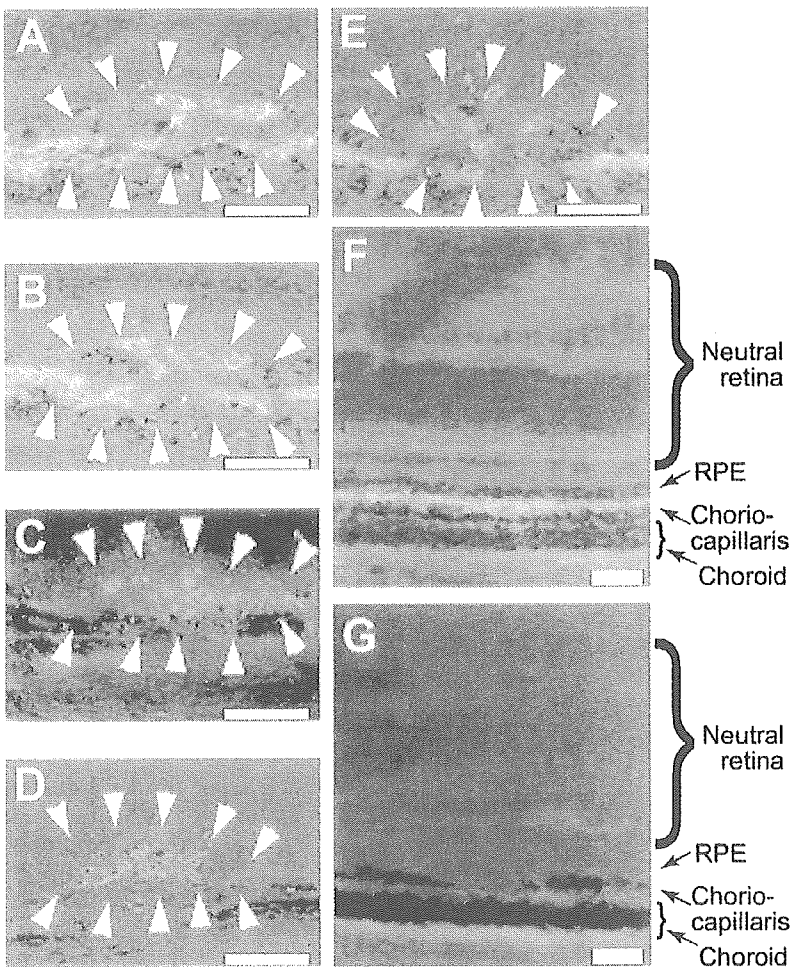

Fig. 3. Accumulation of PIC micelle to CNV lesion. The frozen sections of the CNV lesions were observed under a fluorescent microscopic 1 (A), 4 (B), 24 (C) and 168 (D) h after rats received PIC micelle-incorporated FITC-P(Lys). Note that FITC-P(Lys) initially diffuses to the CNV lesion and choriocapillaris (A,B), and becomes confined to the CNV lesion thereafter (C,D). Bright fluorescence was observed in the CNV lesions up to 168 h (D). One hour after rats received an intravenous injection of free FITC-P(Lys), FITC-P(Lys) distributes to the CNV lesion and choriocapillaris (E). Arrowheads in A–E indicate CNV lesions. Most rats died 1 h after free FITC-P(Lys) administration. In the laser-non-treated eyes, fluorescence was observed in the choriocapillaris 1 h after rats received PIC micelle (F) and the fluorescence became invisible 4 h after the injection of PIC micelle (G). Note that PIC micelle effectively accumulated to the CNV lesion throughout the studied period. Scale bar, 25 μm.

for up to 4 h (Fig. 3A,B). Twenty-four hours after the administration, accumulation of FITC-P(Lys) to the CNV lesion was more evident and fluorescence became invisible outside the photocoagulated lesion including the choroidal and retinal vasculature (Fig. 3C). The fluorescence was observed for up to 168 h (Fig. 3D). In the non-laser-treated eyes, the fluorescence was visible in the choroidal vessels for up to 4 h (Fig. 3F), and the fluorescence became invisible at 24 h and thereafter (Fig. 3G and data not shown). Light microscopic analysis revealed no abnormalities in other retinal structures.

3.2.2. Free FITC-P(Lys) group. Most rats died 1 h after the FITC-P(Lys) administration. When evaluated 1 h after intravenous administration, fluorescence was observed in the CNV lesion and choriocapillaris (Fig. 3E). In order to reduce the toxic effect of free FITC-P(Lys), rats received a lower dose (10 mg per injection) of free FITC-P(Lys). However, all rats died before 2 h after the administration ($n > 10$).

3.3. Concentration of FITC-P(Lys) in the laser-treated eyes

3.3.1. PIC micelle group. FITC-P(Lys) was detected in the retina/choroid from the laser-treated eyes as early as 1 h and the concentration peaked at 4 h and the residual FITC-P(Lys) was still evident 168 h after intravenous administration (Fig. 4). The concentration of FITC-P(Lys) was below the detectable level in the non-laser-treated eyes.

3.3.2. Free FITC-P(Lys) group. When evaluated 1 h after intravenous administration, the concentration of FITC-P(Lys) in the free FITC-P(lys) group was significantly lower compared to that in the PIC micelle group (Fig. 4).

3.4. Concentration of PIC micelle in blood

Fig. 5 shows the concentration of FITC-P(Lys) in blood after a single injection of either free FITC-P(Lys) or PIC micelle encapsulating FITC-P(Lys). The residual amount of FITC-P(Lys) in blood was 5.0, 7.8, 3.8 and 0.5% of the injected dose at 1, 4, 8, and 24 h, respectively, after intravenous injection of PIC micelles encapsulating FITC-P(Lys). After 168 h, it was below the detectable level. The concentration of FITC-P(Lys) in blood was 15% of the injected dose 1 h after free FITC-P(Lys) injection.

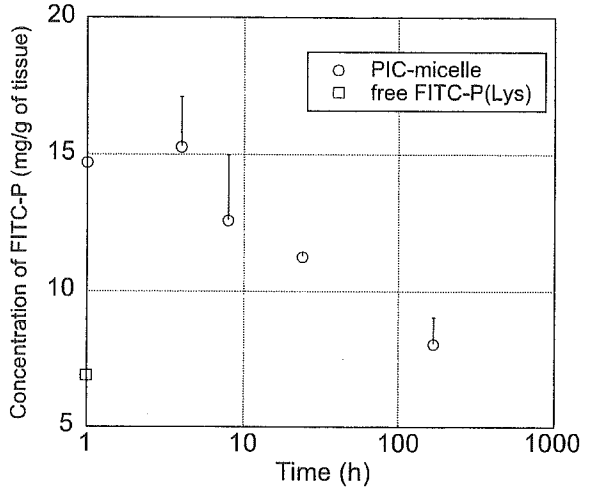

Fig. 4. Concentration of FITC-P(Lys) in retina/choroid. Concentrations of FITC-P(Lys) in retina/choroid after rats received equivalent doses of FITC-P(Lys) of PIC micelle-incorporated FITC-P(Lys). Note that FITC-P(Lys) was detected in retina/choroid from the laser-treated eyes of the PIC micelle group as early as 1 h and the concentration peaked at 4 h and was still evident 18 h after intravenous administration, whereas the concentration of FITC-P(Lys) in the free FITC-P(Lys) group was significantly lower compared to that in the PIC micelle group 1 h after injection. Most rats died 1 h after free FITC-P(Lys) administration. Error bars indicate S.D.

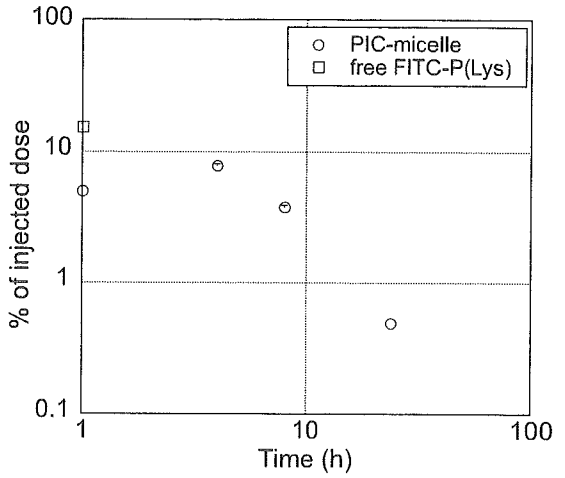

Fig. 5. Concentration of PIC micelle in blood. Concentration of FITC-P(Lys) in blood after rats received 400 μl of free FITC-P(Lys) at a concentration of 5.0 mg/ml or 400 μl of PIC micelles encapsulating 5.0 mg/ml FITC-P(Lys). The residual amount of FITC-P(Lys) in blood was 5.0, 7.8, 3.8 and 0.5% of the injected dose at 1, 4, 8 and 24 h, respectively, after intravenous injection of PIC micelles encapsulating FITC-P(Lys). Most rats died 1 h after free FITC-P(Lys) administration, whereas no rats died after intravenous injection of PIC micelles encapsulating FITC-P(Lys). Error bars indicate S.D.

4. Discussion

In this study, FITC-P(Lys) was retained in the CNV lesion for as long as 168 h after intravenous injection of PIC micelle encapsulating FITC-P(Lys) as demonstrated by histological analysis and confirmed by the measurement of the concentration in the retina/choroid of the laser-treated eyes. Because it was impossible to distinguish free FITC-P(Lys) and FITC-P(Lys) encapsulated into PIC micelle, the data presented here do not address whether FITC-P(Lys) was present in a free form or encapsulated in the PIC micelle. Together with the high mortality rate associated with free FITC-P(Lys) administration, it was not directly proven whether encapsulation of FITC-P(Lys) into PIC micelle enhanced the accumulation of FITC-P(Lys) to the CNV lesions throughout the studied period. However, it was demonstrated that a significantly higher amount of FITC-P(Lys) accumulated to the CNV lesions 1 h after the injection in the PIC micelle group compared to the free FITC-P(Lys) group. It is of note that the amount of FITC-P(Lys) in the non-laser-treated eyes was below the detectable level. In addition, because CNVs are highly permeable similar to the newly formed vessels in solid tumors, it is plausible to speculate that the PIC micelle is likely to accumulate to CNV lesions presumably through the EPR effect. This idea is consistent with recent studies that have demonstrated that macromolecules accumulate in the CNV lesion in rabbits [18].

We have reported that polymeric micelles have long-circulating characteristics [8] and that the stability of PIC micelles

in the blood stream can be controlled by the charge ratio and the length of the poly-amino acid, one of the block copolymers that constitute PIC micelles [19]. In this study, 0.5% of the injected dose was retained in the blood even 24 h after injection of PIC micelle encapsulating FITC-P(Lys). Generally, the concentration of compounds in the blood decreases rapidly to less than 0.1% of the injected dose in a few hours after intravenous injection of low molecular weight compounds such as fluorescein sodium. In fact, the concentration of fluorescein sodium 1 h after intravenous injection was at a non-detectable level (data not shown). Taken together, PIC micelle encapsulating FITC-P(Lys) also have long-circulating characteristics, which is a great advantage to exert the EPR effect.

The concentration of FITC-P(Lys) delivered by PIC micelle to the retina/choroid peaked 4 h after injection, and remained as long as 7 days at a concentration higher than 15 μg/g protein after only one intravenous injection. Because a total of 2 mg FITC-P(Lys) was administered, the total amount of FITC-P(Lys) was approximately 300 ng in the retina/choroid when it was delivered by PIC micelles. As deduced from these results, 0.02% of the injected dose accumulated to and was retained within the retina/choroid for as long as 7 days. In the blood, 5% and 0.5% of the injected dose were retained 1 and 24 h after the injection of PIC micelle, respectively. Thus, the FITC-P(Lys) in blood vs. that in the retina/choroid at 1 and 24 h after the injection was 340:1 and 45:1, respectively, suggesting that PIC micelle could be effectively targeted to the retina/choroid through the EPR effect, in spite of the low concentrations in blood. Moreover, we found that the administration of free FITC-P(Lys) was associated with high mortality, whereas administration of PIC micelles encapsulating FITC-P(Lys) was not. This is in line with previous studies which demonstrated that modification of compounds with a polymeric carrier results in a decreased adverse effect [20]. Our observation supports that the PIC micelle attenuated the adverse effect, although the underlying cause of this lethal toxicity remains to be unraveled. Such characteristics of the PIC micelle are a great advantage to achieve effective targeting of drug while reducing systemic adverse effects.

The concentration of PIC micelles increased in the liver and spleen but gradually decreased in the kidney and lung within 24 h after intravenous injection (data not shown), suggesting that the PIC micelle is mainly eliminated through the spleen.

In summary, it has been demonstrated that the PIC micelle effectively accumulates to the CNV lesion. The distribution of drug-loaded polymeric micelles in the body may be determined mainly by their size and surface properties and is less affected by the properties of loaded drugs if they are embedded in the inner core of the micelles. Since PIC micelles are demonstrated to be able to reserve a variety of drugs, enzymes [21] and DNA in the core and can serve as non-viral gene delivery vectors [9,19,22], we believe that PIC micelles have great potential for achieving effective drug targeting to CNV.

References

[1] Ferris III, F.L., Fine, S.L. and Hyman, L. (1984) Arch. Ophthalmol. 102, 1640–1642.
[2] Bressler, N.M., Bressler, S.B. and Fine, S.L. (1988) Surv. Ophthalmol. 32, 375–413.
[3] Macular Photocoagulation Study Group (1991) Arch. Ophthalmol. 109, 1242–1257.
[4] Treatment of age related macular degeneration with photodynamic therapy (TAP) Study Group (1999) Arch. Ophthalmol. 117, 1329–1345.
[5] Ciulla, T.A., Danis, R.P. and Harris, A. (1998) Surv. Ophthalmol. 43, 134–146.
[6] Hunt, D.W. and Margaron, P. (2003) IDrugs 6, 464–469.
[7] Kimura, H., Yasukawa, T., Tabata, Y. and Ogura, Y. (2001) Adv. Drug Deliv. Rev. 52, 79–91.
[8] Kataoka, K., Harada, A. and Nagasaki, Y. (2001) Adv. Drug Deliv. Rev. 47, 113–131.
[9] Kakizawa, Y. and Kataoka, K. (2002) Adv. Drug Deliv. Rev. 54, 203–222.
[10] Matsumura, Y. and Maeda, H. (1986) Cancer Res. 46, 6387–6392.
[11] Nakanishi, T. et al. (2001) J. Control. Release 74, 295–302.
[12] Nishiyama, H., Kato, Y., Sugiyama, Y. and Kataoka, K. (2001) Pharm. Res. 18, 1035–1041.
[13] Kataoka, K., Matsumoto, T., Yokoyama, M., Okano, T., Sakurai, Y., Fukushima, S., Okamoto, K. and Kwon, G.S. (2000) J. Control. Release 64, 143–153.
[14] Nishiyama, N. and Kataoka, K. (2003) Adv. Exp. Med. Biol. 519, 155–177.
[15] Harada, A. and Kataoka, K. (1995) Macromolecules 28, 5294–5299.
[16] Yanagi, Y., Tamaki, Y., Obata, R., Muranaka, K., Homma, N., Matsuoka, H. and Mano, H. (2002) Invest. Ophthalmol. Vis. Sci. 43, 3495–3499.
[17] Yanagi, Y., Tamaki, Y., Inoue, Y., Obata, R., Muranaka, K. and Homma, N. (2003) Invest. Ophthalmol. Vis. Sci. 44, 751–754.
[18] Yasukawa, T., Kimura, H., Tabata, Y., Miyamoto, H., Honda, Y., Ikada, Y. and Ogura, Y. (1999) Invest. Ophthalmol. Vis. Sci. 40, 2690–2696.
[19] Harada-Shiba, M., Yamauchi, K., Harada, A., Takamisawa, I., Shimokado, K. and Kataoka, K. (2002) Gene Ther. 9, 407–414.
[20] Mizumura, Y. et al. (2001) Jpn. J. Cancer Res. 92, 328–336.
[21] Harada, A. and Kataoka, K. (2001) J. Control. Release 72, 85–91.
[22] Harada, A., Togawa, H. and Kataoka, K. (2001) Eur. J. Pharm. Sci. 13, 35–42.

11. 強度近視に伴う中心窩分離に対する硝子体手術適応に関する考察

生野恭司[1)]、佐柳香織[1)]、十河　薫[1)]、沢　美喜[1)]、坂口裕和[1)]、大島佑介[1)]、
五味　文[1)]、瓶井資弘[1)]、日下俊次[1)]、田野保雄[1)]、大路正人[2)]
([1)] 大阪大、[2)] 滋賀医大)

研究要旨　強度近視に対し近年、硝子体手術が積極的に行われるようになったがその適応や手術の効果については未だ議論の余地は多い。今回中心窩分離症の硝子体手術例を振り返り、その手術効果および手術予後に関連する因子を検討した。対象は2001年から大阪大学医学部附属病院にて硝子体手術を行った中心窩分離症例26例28眼である。術式は有水晶体眼では水晶体超音波乳化吸引術と眼内レンズ挿入術を行い、後部硝子体剥離作成、内境界膜剥離、ガスタンポナーデである。術後全例で中心窩分離症は消失し、網膜は復位したが、1眼が術3ヶ月後に黄斑円孔を発症した。術後6ヶ月の時点で2段階以上の視力改善を得たものは17眼（61%）、不変が9眼（32%）、2段階以上の悪化が2眼（7%）であった。また、術前視力は術後視力と強い正の相関を示した（P<0.01）。術前視力別に検討すると術前視力が0.1未満であったものは10眼中9眼（90%）、0.1以上0.4未満であったものは13眼中8眼（62%）、0.4以上のものは5眼中0眼（0%）で術後2段階以上の視力改善を得た。術前の発症期間と術後の視力改善は統計学的に有意な負の相関を示した(P<0.05)が、発症期間と術後視力、年齢と術後視力および視力改善に関しては有意な相関は認めなかった。多くの症例で視力改善が得られる本術式は高度近視眼に伴う中心窩分離症に対して有効であると考えられる。良好な術後視力を期待するのであれば視力低下が軽度である発症早期に間に行うのが望ましいが、視力改善の面では視力が良好なほど不利になるため、今後手術の適応に関してはさらに症例の追加と検討が必要であると思われる。

A．研究目的

強度近視は未だ社会的失明原因の上位を占めている。強度近視眼では眼軸長の極端な延長に伴い、網脈絡膜萎縮、黄斑円孔網膜剥離など特異的な疾病が見られる。中心窩分離症はそのひとつで1950年代に「黄斑円孔のない後極部網膜剥離」として当初報告された。その後光干渉断層計など機器の発達により網膜剥離ではなく網膜分離であること、単一病態ではなく形態的にさまざまなSubtypeが存在することなどが理解されるようになった[1,2)]。分離症を放置した場合、難治性の黄斑円孔網膜剥離に進展する可能性もある[2,3)]。原因は今のところ不明だが、硝子体牽引、網膜血管牽引、黄斑前膜、内境界膜の伸展不全などが考えられている

[4-6]。治療としては後部硝子体剥離作成、内境界膜剥離、ガスタンポナーデを含む硝子体手術が積極的に行われているが[7,8]、その歴史は浅く、その効果や手術の成績に関与する因子についてまだまだ不明な点も多い。本研究では当施設で行った中心窩分離症の硝子体手術例を後ろ向きに調査し、硝子体手術の効果と安全性、手術予後に関与する因子について検討を行った。

B．研究方法および倫理面への配慮

対象は2001年から大阪大学医学部附属病院にて硝子体手術を行った中心窩分離症例26例28眼（中心窩剥離型21眼、分層円孔型8眼）である。平均年齢は63.9歳、平均眼軸長は29.1mmであった。術式は型のごとく有水晶体眼では水晶体超音波乳化吸引術と眼内レンズ挿入術を行い、トリアムシノロンで硝子体を可視化した後に後部硝子体剥離作成、インドシアニングリーン染色による内境界膜剥離、ガスタンポナーデを行った。これら症例の性別、年齢、術前発症期間、術前術後視力を後ろ向きに調査した。最低術後経過観察期間が6ヶ月未満のものは除外した。また、手術の際には患者に手術のリスク等を十分に説明の上、インフォームドコンセントを獲得して行った。

C．研究結果

術後全例で中心窩分離症は消失し、網膜は復位したが、1眼が術3ヶ月後に黄斑円孔を発症した。続発性網膜剥離や硝子体出血など重篤な併発症をきたした症例はなかった。術後6ヶ月の時点で2段階以上の視力改善を得たものは17眼（61%）、不変が9眼（32%）、2段階以上の悪化が2眼（7%）であった。また、術前視力は術後視力と強い正の相関を示した（$P<0.01$）。術前視力別に検討すると術前視力が0.1未満であったものは10眼中9眼（90%）、0.1以上0.4未満であったものは13眼中8眼（62%）、0.4以上のものは5眼中0眼（0%）で術後2段階以上の視力改善を得た。中心窩剥離型の術前術後視力は分層円孔型よりのそれよりもやや低い傾向があり、視力改善は逆に良好であったが、有意な差は見られなかった。術前の発症期間と術後の視力改善は統計学的に有意な負の相関を示した（$P<0.05$）が、発症期間と術後視力、年齢と術後視力および視力改善に関しては有意な相関は認めなかった。

D．考察

本術式は重篤な併発症の可能性は極めて低かったことから安全性が高く、また60%を超える症例で術後視力改善が得られたことから有用な治療法であることを示唆している。良好な術後視力を期待するのであれば視力低下が軽度である発症早期に行うのが望ましいが、視力改善の面では術前視力が良好なほど不利になるため、手術適応に関してはさらに症例の追加と検討が必要であると思われる。また、発症期間が3年前後の症例でも手術により視力改善の可能性がある。

E．結論

中心窩分離症に対する硝子体手術は有用である。手術適応など詳細な点については今後さらに検討を要する。

F．健康危険情報

なし

G．研究発表

1．論文発表

1. Bando H, Ikuno Y, Choi JS, Tano Y, Yamanaka I, Ishibashi T: Ultrastructure of internal limiting membrane in myopic foveoschisis. Am J Ophthalmol. 139: 197-199, 2005.
2. Ikuno Y, Gomi F, Tano Y: Potent retinal arteriolar traction as a possible cause of myopic foveoschisis. Am J Ophthalmol.139:462-467, 2005.
3. Sayanagi K, Ikuno Y, Gomi F, Tano Y: Retinal vascular microfolds in highly myopic eyes. Am J Ophthalmol. 139: 658-663, 2005.

2．学会発表

なし

H．知的財産権の出願・登録状況

1．特許取得

なし

2．実用新案登録

なし

3．その他

なし

I．参考文献

1. Takano M, Kishi S: Foveal retinoschisis and retinal detachment in severely myopic eyes with posterior staphyloma. Am J Ophthalmol. 128: 472-476, 1999.
2. Benhamou N, Massin P, Haouchine B, Erginay A, Gaudric A: Macular retinoschisis in highly myopic eyes. Am J Ophthalmol 133: 794-800, 2002.
3. Ikuno Y and Tano Y: Early macular holes with retinoschisis in highly myopic eyes. Am J Ophthalmol 136: 741-744, 2003.
4. Sakaguchi H, Ikuno Y, Choi JS, Ohji M, Tano T: Multiple components of epiretinal tissues detected by triamcinolone and indocyanine green in macular hole and retinal detachment as a result of high myopia. Am J Ophthalmol. 138: 1079-1081, 2004.
5. Bando H, Ikuno Y, Choi JS, Tano Y, Yamanaka I, Ishibashi T: Ultrastructure of internal limiting membrane in myopic foveoschisis. Am J Ophthalmol. 139: 197-199, 2005.
6. Ikuno Y, Gomi F, Tano Y: Potent retinal arteriolar traction as a possible cause of myopic foveoschisis. Am J Ophthalmol. 139: 462-467, 2005.
7. Kobayashi H, Kishi S: Vitreous surgery for highly myopic eyes with foveal detachment and retinoschisis. Ophthalmology 110: 1702-1707, 2003.
8. Ikuno Y, Sayanagi K, Ohji M, et al: Vitrectomy and internal limiting membrane peeling for myopic foveoschisis. Am J Ophthalmol 137: 719-724, 2004.

Potent Retinal Arteriolar Traction as a Possible Cause of Myopic Foveoschisis

YASUSHI IKUNO, MD, FUMI GOMI, MD, AND YASUO TANO, MD

• PURPOSE: To report retinal microfold formation after vitrectomy for myopic foveoschisis (MF).
• DESIGN: Prospective observational study.
• METHODS: We observed 21 eyes of 17 patients who had undergone vitrectomy for MF with optical coherence tomography (OCT) in this institutional study. We also evaluated the three-dimensional retinal architecture using the OCT-ophthalmoscope in selected cases. Vitrectomy included core vitrectomy, vitreous cortex removal, internal limiting membrane (ILM) peeling with indocyanine green, and gas tamponade.
• RESULTS: Horizontal linear folds were commonly observed postoperatively. The folds, which were 1,000 to 2,000 μm superior, inferior, or both superior and inferior to the fovea, were detected only by OCT and not by conventional slit-lamp-based biomicroscopy. The microfolds were found in only five eyes (24%) 1 month postoperatively. The incidence increased over time, however, and a microfold was detected in nine eyes (43%) 3 months after surgery and in 13 (62%) 6 months after surgery. OCT-ophthalmoscope examination confirmed the location of the microfold coincided exactly with that of retinal arteriole. The presence of microfolds was not significantly related to the postoperative visual acuity.
• CONCLUSIONS: Retinal microfolds are common in eyes with MF after vitrectomy with ILM peeling, and they seem to be generated as the result of insufficient flexibility of the sclerotic retinal arteriole during axial length elongation in highly myopic eyes. This finding suggests that the inward tractional force on the retina along the arteriole may be closely related to the pathogenesis of vitreoretinal diseases specific to high myopia, including MF or paravascular microhole formation. (Am J Ophthalmol 2005;139:462–467. © 2005 by Elsevier Inc. All rights reserved.)

Accepted for publication Sep 30, 2004.
From the Department of Ophthalmology, Osaka University Medical School, Osaka, Japan.
Inquiries to Yasushi Ikuno, MD, Department of Ophthalmology, Room E7, Osaka University Medical School, 2-2 Yamadaoka, Suita 565–0871 Japan; fax: (+81) 6-6879-3458; e-mail: ikuno@ophthal.med.osaka-u.ac.jp

MYOPIC FOVEOSCHISIS (MF) IS NOT UNCOMMON IN highly myopic eyes and reportedly is associated with posterior staphyloma formation.[1,2] In addition, MF leads to macular hole formation, at least in some cases.[3,4] Vitrectomy, internal limiting membrane (ILM) peeling and gas tamponade are useful treatments to attain foveal reattachment and consequent visual improvement in cases without macular holes.[5–7]

ILM peeling provides redundancy of the retinal surface. However, clinical and laboratory observation has shown that in certain situations indocyanine green (ICG)-assisted ILM peeling may be harmful,[8,9] and it is controversial whether ILM peeling is beneficial for patients. Other investigators have suggested that the ILM can be the primary component that generates tractional force at the posterior retina in highly myopic eyes,[10] although there is poor evidence to support this hypothesis.

We observed eyes that underwent vitrectomy, ILM peeling, and gas tamponade for MF using optical coherence tomography (OCT) and OCT-ophthalmoscope to evaluate the retinal status after surgery. We found that microfolds developed in the retina in these eyes after surgery. The location of the microfolds coincided with that of the retinal arteriole, indicating that ILM peeling may have disclosed the inward tractional force of the sclerotic retinal arteriole because of insufficient flexibility during elongated axial length.

PATIENTS AND METHODS

Patients. Twenty-one eyes of 17 patients who underwent vitrectomy for MF were included in this study. Eyes with a macular hole or an early macular hole were also included.[4,11] Patients with postoperative follow-up of less than 6 months were excluded. The preoperative appearance of MF was based on the classification of Benhamou and associates[3] with slight modification, including foveal detachment, lamellar hole, cystic MF, and macular hole. Thirteen eyes (62%) had a foveal detachment, 4 eyes (19%) a lamellar hole, and 4 eyes (19%) a macular hole. No eyes in this study had the cystic type of MF. Informed consent was obtained from all the patients.

0002-9394/05/$30.00
doi:10.1016/j.ajo.2004.09.078

TABLE 1. Patient Demographic Data and the Presence or Absence of Retinal Microfolds After Vitrectomy for Myopic Foveoschisis

Case No.	Age/Gender	R/L	Type	Postoperative (months) 1	3	6	12	Comments
1	65/F	R	Foveal detachment	N	N	Y	N	
2	65/F	R	Foveal detachment	N	Y	Y	Y	
2	65/F	L	Foveal detachment	N	Y	Y	Y	
3	51/F	R	Foveal detachment	N	N	N	Y	
4	48/F	R	Macular hole	N	Y	Y	Y	Macular hole remained after additional vitrectomy
4	48/F	L	Foveal detachment	N	N	Y	Y	
5	65/F	R	Foveal detachment	N	Y	N	Y	
6	54/M	R	Foveal detachment	Y	Y	Y	Y	
7	73/F	R	Foveal detachment	N	N	N	N	
7	73/F	L	Macular hole	N	N	N	N	Macular hole closed
8	80/F	R	Macular hole	N	N	Y	NA	Macular hole remained
9	59/F	R	Foveal detachment	N	N	Y	Y	
10	59/F	R	Macular hole	Y	Y	Y	Y	Macular hole remained after additional vitrectomy
11	79/F	R	Lamellar hole	N	N	N	N	
12	67/F	R	Foveal detachment	N	N	N	N	
12	67/F	L	Foveal detachment	N	N	Y	Y	
13	66/F	R	Lamellar hole	N	N	N	N	
14	55/F	L	Lamellar hole	N	N	N	N	
15	62/F	R	Lamellar hole	Y	Y	Y	Y	
16	72/F	R	Macular hole	Y	Y	Y	Y	Macular hole closed after additional gas injection
17	65/M	R	Foveal detachment	Y	Y	Y	Y	

M = male; F = female; Y = yes; N = no; NA = not available.

Surgical Procedure. Vitrectomy was performed according to the method previously described.[7] Phacoemulsification and simultaneous intraocular lens implantation were performed in 17 phakic eyes (81%). After core vitrectomy, the vitreous cortex was removed using triamcinolone acetonide[12] (Kenacort-A, Bristol-Myers Squibb, New York, New York, USA) and a diamond-dusted membrane scraper,[13] and an ILM of 2 to 3 disk diameters was peeled after staining with 5 mg/ml of ICG (Dai-ichi Pharmaceutical, Tokyo, Japan). The ICG was sprayed onto the retina through a 27-G blunt needle, and the excess ICG was aspirated immediately with a vitrectomy cutter. Finally, the vitreous fluid was totally exchanged with air, and gas tamponade was performed. Sixteen percent perfluoropropane was used in 17 eyes (81%), 20% sulfur hexafluoride in 3 (14%), and room air in 1 (5%). The patients were instructed to maintain a prone position for 1 week postoperatively.

Examination. The retinal status was evaluated with OCT (Humphrey, Dublin, California, USA) and OCT-ophthalmoscope (OTI, Toronto, Canada).[14] OCT scans were performed using the default setting of the crosshairs mode, which scans the retina horizontally and vertically (scan length, 5.65 mm). OCT examinations were performed 1, 3, 6, and 12 months after surgery.

The OCT-ophthalmoscope provides simultaneously "en face" (C-scan) images and cross-sectional (B-scan) images of the retina. The procedure was performed according to the manufacturer's instructions with the default setting at the 6-month follow-up visit in selected cases. Scanning laser ophthalmoscopic (SLO) images of the retinal surface were obtained simultaneously to identify the location of the microfolds detected on the C-scan images. The location on the retina was determined by overlaying the C-scan image onto the SLO image with the same section of the retina with default application of the system.

Other routine examinations such as slit-lamp-based biomicroscopic observation, fundus photography, and best-corrected visual acuity measurements (BCVA) also were performed at each follow-up visit.

Statistical Analysis. Statistical analysis was performed using the commercially available application Sigma Stat (SPSS, Chicago, Illinois, USA) to detect statistically significant differences. $P < .05$ was considered significant.

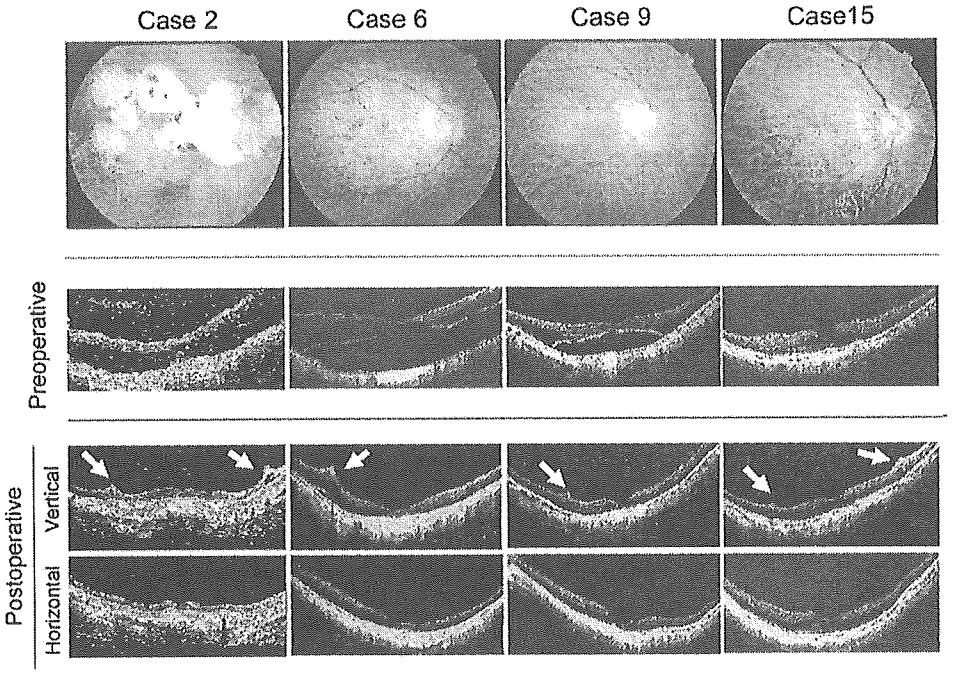

FIGURE 1. Typical appearance of a microfold after vitrectomy for myopic foveoschisis (MF). (Top row) Postoperative fundus photographs of the macula; (second row) preoperative optical coherence tomographic data (OCT); (third and fourth rows) postoperative vertical and horizontal OCT scans 6 months postoperatively. In all four cases, MF is present preoperatively. Cases 2, 6, and 9 have the foveal detachment type, and case 15 has the lamellar hole type. The fovea was successfully reattached postoperatively in three cases with the foveal detachment type, and the foveal architecture returned to normal in case 15. A retinal microfold is detected by vertical OCT scan postoperatively (arrows), however. The microfold is unclear in the fundus photograph and was not detected by conventional microscopy. It was detected only in the OCT vertical scan, not in the horizontal scan, after surgery. Folds are observed on either side (cases 6 and 9) or on both sides (cases 2 and 15) of the fovea.

RESULTS

THE DEMOGRAPHIC DATA FROM ALL PATIENTS (15 WOMEN, 2 men) and the presence or absence of microfolds at the time of OCT are shown in the Table. The mean age of the patients was 63.8 ± 9.0 (mean ± SD) years (range, 48-80 years). Microfolds were found in only five eyes (24%) 1 month postoperatively. The incidence increased over time, however, and microfolds were detected in nine eyes (43%) 3 months postoperatively and 13 eyes (62%) 6 months postoperatively. After 12 months, OCT data were unavailable for one eye (5%, case 8); however, microfolds were observed in 13 (65%) of the remaining 20 eyes.

The foveal architecture returned to normal in all eyes with a foveal detachment and a lamellar hole. The macular holes closed in one (20%) of five eyes after the initial vitrectomy and persisted in the other four eyes (80%). Of the four eyes, the macular holes closed with additional gas injection in one eye (case 16); however, the macular hole did not close even with vitrectomy, including extended ILM peeling and gas tamponade in case 10 and the right eye of case 4. One patient refused additional treatment, and the macular hole remained open (case 8). The BCVA was 0.125 median preoperative and 0.3 postoperatively. The BCVA improved more than 2 lines in 13 (62%) eyes, remained unchanged in 8 (38%), and did not worsen in any (0%).

Typical microfolds in MF are shown in Figure 1. Because of their size, the microfolds could not be detected during a conventional fundus examination (Figure 1, top row) and were detected only with OCT. The folds were detected by vertical scan but not by horizontal scan, indicating that the folds were always generated in a horizontal direction (Figure 1, second, third, and fourth rows). The microfolds, which were superior to, inferior to, or on both sides of the fovea, were 1,000 to 2,000 μm from the fovea based on the scan length of 5.65 mm.

Typically, the microfolds began to develop 1 month postoperatively and continued to develop (Figure 2). Microfolds were more obvious 3 or 6 months postoperatively compared with 1 month postoperatively. The microfolds persisted until the final visit (6 or 12 months postoperatively) in all eyes except case 1, in which the microfolds resolved between 6 and 12 months postoperatively probably because of resolution of the intraretinal fluid.

OCT-ophthalmoscope examination confirmed the presence of microfolds (Figure 3). C-scan images of the examination provided more information, including the

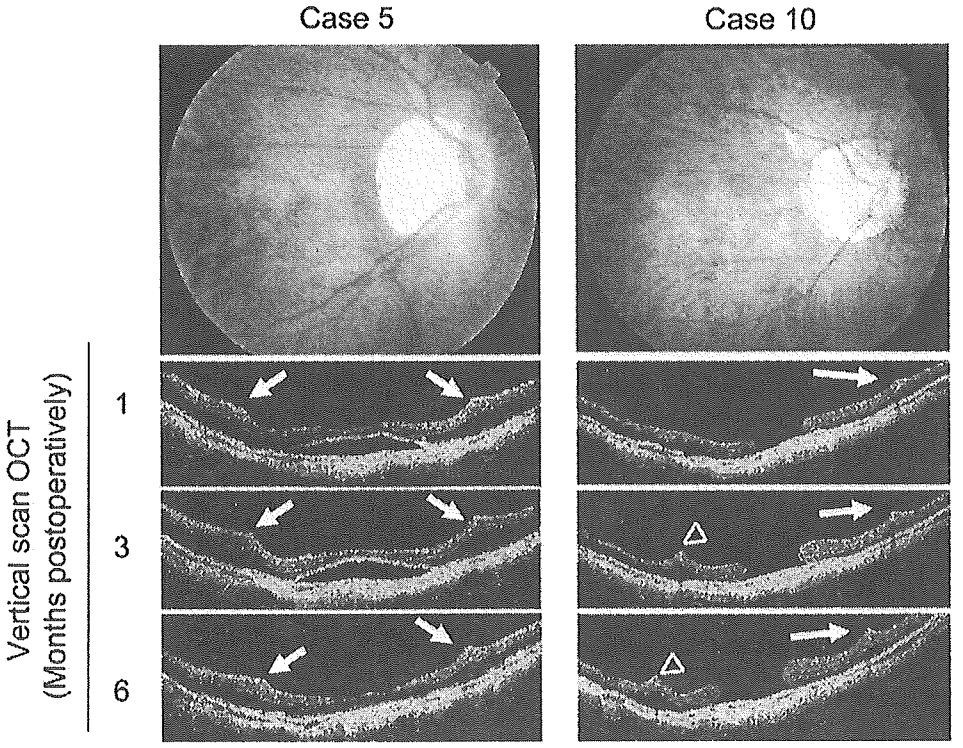

FIGURE 2. Typical time course of microfolds after vitrectomy for myopic foveoschisis. (Top row) Macular fundus photograph and (second, third, and fourth rows) postoperative optical coherence tomography scan results in two cases. The number indicates the number of months after surgery, and the OCT scan is always vertical. (case 5) Two microfolds superior and inferior to the foveal center are present 1 month after surgery (arrows); however, both are more prominent 3 months postoperatively (arrows). The microfolds have decreased somewhat 6 months after surgery, perhaps due to resolution of MF (arrows). (case 10) A microfold superior to the fovea appears 1 month after surgery (arrow). The macular hole is open. This microfold is more prominent 3 months after surgery (arrow), and another microfold is on the other side of the fovea (arrowhead). Both microfolds persist and are somewhat more prominent 6 months after surgery (arrow and arrowhead).

direction and showed that retinal microfolds were horizontal in orientation (Figure 3, A–C, top right). To identify the accurate location of the microfolds, we positioned the C-scan images (Figure 3, A–C, top right) of the OCT-ophthalmoscope over the SLO images taken simultaneously (Figure 3, A–C, top left). The merged image showed that the location of microfolds coincided exactly with the retinal vessels (Figure 3, A–C, bottom left). Color fundus photographs showed that the vessels were always the retinal arteriole but not the venule (Figure 3, A–C, bottom right). Thus, the microfolds coincided exactly with the retinal arteriole, and this was why the microfolds were always horizontal in the OCT images.

When we compared the BCVA 6 months postoperatively between eyes with microfolds and those without, there was no significant difference ($P = .67$ by t-test).

DISCUSSION

TO THE BEST OF OUR KNOWLEDGE, NO REPORTS WITH similar findings have been published. One report described retinal folds after vitrectomy for X-linked retinoschisis; however, the appearance of the folds was different from those in our study.[15] As mentioned earlier, it is difficult to identify microfolds with conventional methods such as slit-lamp biomicroscopy. Thus, the recent advances in instrumentation, including OCT and OCT-ophthalmoscope, for examining details of the retinal architecture may have enabled us to detect the folds in our cases.

It is generally accepted that ILM peeling provides retinal redundancy, which is believed to be the main reason for enhanced macular hole closure. Although we need to observe more patients, we believe that retinal redundancy due to ILM peeling allowed microfold development. We found that the microfolds coincided exactly with the retinal arteries, which leads us to hypothesize that retinal redundancy after ILM peeling disclosed the inward traction of the sclerotic retinal arteriole due to insufficient flexibility after axial length elongation or posterior staphyloma formation (or both) in these eyes. Microfolds are rarely observed in nonvitrectomized eyes, probably because the retina is not redundant in those eyes, and the potent tractional force does not develop in the presence of the ILM. The mechanism of microfold formation is still un-

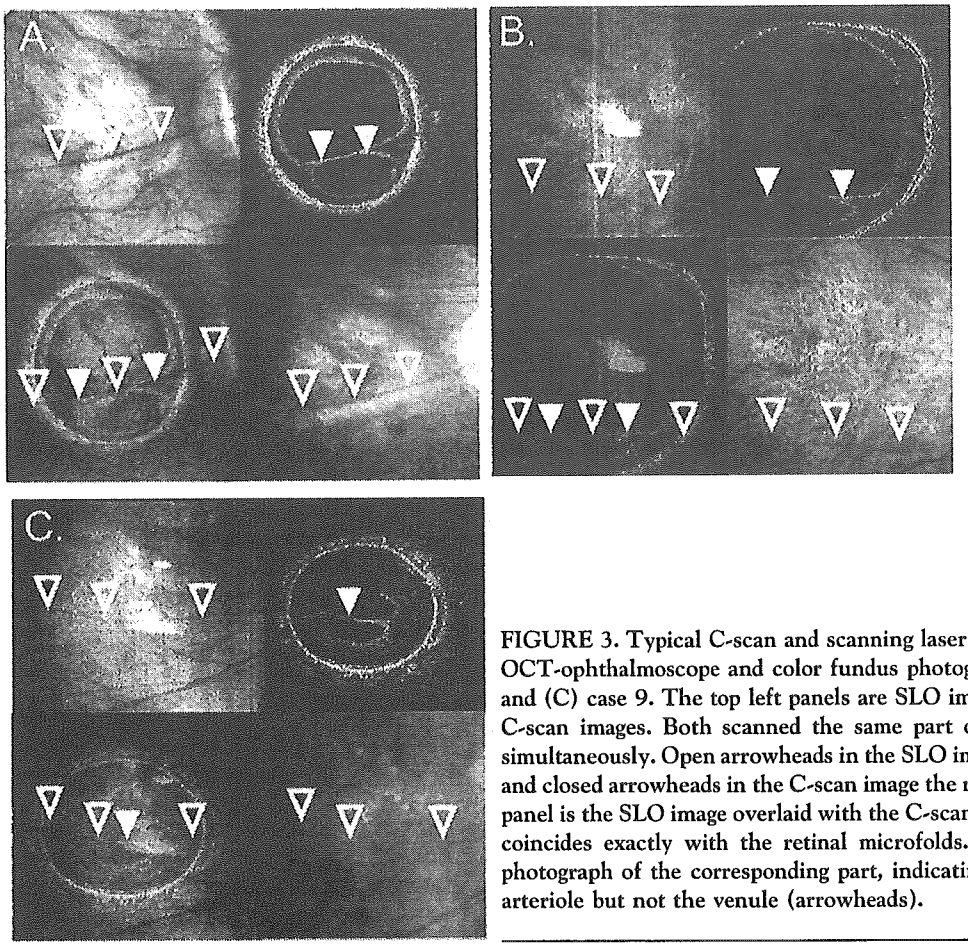

FIGURE 3. Typical C-scan and scanning laser ophthalmoscopic (SLO) image of OCT-ophthalmoscope and color fundus photograph of (A) case 17, (B) case 6, and (C) case 9. The top left panels are SLO images, and the top right panels are C-scan images. Both scanned the same part of the retina and were examined simultaneously. Open arrowheads in the SLO images indicate the retinal arteriole, and closed arrowheads in the C-scan image the retinal microfolds. The bottom left panel is the SLO image overlaid with the C-scan image. Note that retinal arteriole coincides exactly with the retinal microfolds. Bottom right is a color fundus photograph of the corresponding part, indicating that the vessel was the retinal arteriole but not the venule (arrowheads).

known and another possible mechanism—for instance, retinal architectural changes by Müller cells—cannot be ruled out.

The clinical relevance of microfold formation and potent tractional force is unknown. One possibility is that the tractional force may be related to the pathogenesis of foveoschisis. In our experience, we rarely observe vitreous tractional force during surgery, which is typically seen in macular traction syndrome in nonmyopic eyes. This leads us to hypothesize that factors other than vitreous traction can result in MF, and we believe this tractional force at the retinal arteriole might be a cause. The retina may be lifted off the retinal pigment epithelium due to this "retinal arteriolar" tractional force. Surgical removal of the ILM provides retinal redundancy and may allow a retinal structure other than the arteriole (perhaps the foveal center) to reattach to the retinal pigment epithelium.

We specifically observed microfolds in eyes with MF after vitrectomy. We also reviewed the OCT images from 16 patients with a macular hole and retinal detachment in highly myopic eyes. These eyes have been reported previously.[16] However, the microfolds as observed in this study were not found in any of the 16 eyes (data not shown), indicating that microfolds are specific to MF and not to highly myopic eyes that underwent vitrectomy. This also supports the hypothesis that retinal arteriolar traction can cause MF. A published report described the spontaneous resolution of MF, however.[17] Thus, the contribution of vitreous traction cannot be ruled out.

Another possible effect of this tractional force is that it may cause posterior paravascular break formation that sometimes occurs in highly myopic eyes.[18–20] Paravascular retinal breaks in highly myopic eyes are typically small and round. Vitreous traction at the site of paravascular vitreoretinal adhesion is believed to be the main cause of retinal rarefaction formation, resulting in retinal break formation from posterior vitreous detachment.[21] However, this was not commonly observed in the posterior retina in highly myopic eyes. Taken together, retinal arteriolar traction in highly myopic eyes may cause paravascular retinal break formation.

The presence of microfolds does not seem to affect the postoperative vision. In this study, most patients had improved BCVA despite the presence of microfolds. The foveal architecture also returned to normal in all eyes with a foveal detachment and the lamellar hole. Although microperimetry was not performed in this study, it seems that the effect of microfold formation is limited because microfolds are small and there are other factors, such as retinal pigment epithelium and choroidal atrophic

changes, that could affect vision. Moreover, the location of the microfolds coincided exactly with the retinal arteriole.

As we mentioned earlier, three factors, including a highly myopic eye, ILM peeling, and MF are essential for microfold formation. Microfolds are a newly recognized entity. Longer-term follow-up and more detailed observation and evaluation are necessary to characterize microfolds fully.

REFERENCES

1. Takano M, Kishi S. Foveal retinoschisis and retinal detachment in severely myopic eyes with posterior staphyloma. Am J Ophthalmol 1999;128:472–476.
2. Baba T, Ohno-Matsui K, Futagami S, et al. Prevalence and characteristics of foveal retinal detachment without macular hole in high myopia. Am J Ophthalmol 2003;135:338–342.
3. Benhamou N, Massin P, Haouchine B, Erginay A, Gaudric A. Macular retinoschisis in highly myopic eyes. Am J Ophthalmol 2002;133:794–800.
4. Ikuno Y, Tano Y. Early macular holes with retinoschisis in highly myopic eyes. Am J Ophthalmol 2003;136:741–744.
5. Kanda S, Uemura A, Sakamoto Y, Kita H. Vitrectomy with internal limiting membrane peeling for macular retinoschisis and retinal detachment without macular hole in highly myopic eyes. Am J Ophthalmol 2003;136:177–180.
6. Kobayashi H, Kishi S. Vitreous surgery for highly myopic eyes with foveal detachment and retinoschisis. Ophthalmology 2003;110:1702–1707.
7. Ikuno Y, Sayanagi K, Ohji M, et al. Vitrectomy and internal limiting membrane peeling for myopic foveoschisis. Am J Ophthalmol 2004;137:719–724.
8. Haritoglou C, Gandorfer A, Gass CA, Schaumberger M, Ulbig MW, Kampik A. Indocyanine green-assisted peeling of the internal limiting membrane in macular hole surgery affects visual outcome: a clinicopathologic correlation. Am J Ophthalmol 2002;134:836–841.
9. Yam HF, Kwok AK, Chan KP, et al. Effect of indocyanine green and illumination on gene expression in human retinal pigment epithelial cells. Invest Ophthalmol Vis Sci 2003;44:370–377.
10. Kuhn F. Internal limiting membrane removal for macular detachment in highly myopic eyes. Am J Ophthalmol 2003; 135:547–549.
11. Akiba J, Konno S, Sato E, Yoshida A. Retinal detachment and retinoschisis detected by optical coherence tomography in a myopic eye with a macular hole. Ophthalmic Surg Lasers 2000;31:240–242.
12. Peyman GA, Cheema R, Conway MD, Fang T. Triamcinolone acetonide as an aid to visualization of the vitreous and the posterior hyaloid during pars plana vitrectomy. Retina 2000;20:554–555.
13. Oshima Y, Ikuno Y, Motokura M, Nakae K, Tano Y. Complete epiretinal membrane separation in highly myopic eyes with retinal detachment resulting from a macular hole. Am J Ophthalmol 1998;126:669–676.
14. Podoleanu AG, Dobre GM, Cucu RG, et al. Combined multiplanar optical coherence tomography and confocal scanning tomography. J Biomed Opt 2004;9:86–93.
15. Phillips P, Hutchins RK. Development of a large macular fold following surgical repair of a traction retinal detachment in a child with x-linked retinoschisis. Retina 2003;23:855–856.
16. Ikuno Y, Sayanagi K, Oshima T, et al. Optical coherence tomographic findings of macular holes and retinal detachment after vitrectomy in highly myopic eyes. Am J Ophthalmol 2003;136:477–481.
17. Polito A, Lanzetta P, Del Borrello M, Bandello F. Spontaneous resolution of a shallow detachment of the macula in a highly myopic eye. Am J Ophthalmol 2003;135:546–547.
18. Favre M. Trous parapapillaires comme cause du décollement de la rétine. Ophthalmologica (Basel) 1954;127: 351–356.
19. Phillips CI, Dobbie JG. Posterior staphyloma and retinal detachment. Am J Ophthalmol 1963;55:332–335.
20. Malbran ES, Dodds R. Different types of holes and their significance. Mod Probl Ophthalmol 1967;5:170–186.
21. Spencer LM, Foos RY. Paravascular vitreoretinal attachments. Role in retinal tears. Arch Ophthalmol 1970;84:557–564.